A High Temperature Superconductor notch filter for the Sardinia Radio Telescope

Pietro Bolli[1*], Luca Cresci[1], Frederick Huang[2], Sergio Mariotti[3], Dario Panella[1]

[1] Arcetri Astrophysical Observatory, National Institute for Astrophysics, Largo E. Fermi 5, Florence, Italy
[2] School of EESE, University of Birmingham, Edgbaston, Birmingham, B15 2TT, UK
[3] Institute of Radio Astronomy, National Institute for Astrophysics, via P. Gobetti 101, Bologna, Italy
[*] pbolli@arcetri.inaf.it

Abstract: A High Temperature Superconductor filter operating in the C-band between 4200 and 5600 MHz has been developed for one of the radio astronomical receivers of the Sardinia Radio Telescope. The motivation was to attenuate an interference from a weather radar at 5640 MHz, whose power level exceeds the linear region of the first active stages of the receiver. A very sharp transition after the nominal maximum passband frequency is reached by combining a 6th order band-pass filter with a 6th order stop-band. This solution is competitive with an alternative layout based on a cascaded triplet filter. Three units of the filter have been measured with two different calibration approaches to investigate pros and cons of each, and data repeatability. The final performance figures of the filters are: ohmic losses of the order of 0.15-0.25 dB, matching better than -15 dB, and -30 dB attenuation at 5640 MHz. Finally, a more accurate model of the connection between external connector and microstrip shows a better agreement between simulations and experimental data.

Keywords: Radio Telescope; Radio Frequency Interference; High Temperature Superconductor; Microwave Filters; Scattering parameters; Vector Network Analyser.

1. Introduction

The Sardinia Radio Telescope (SRT) is a 64-m radio telescope inaugurated in 2013 and operated by the National Institute for Astrophysics (INAF) [1]. The first-light of the SRT was performed with a front-end receiver covering the frequency range between 5700 to 7700 MHz [2]. As a part of the second generation receivers, the development of a new receiver to cover the remaining part of the C-band, from 4200 to 5600 MHz (28.6% relative bandwidth), started in 2015. The main scientific drivers for this receiver are Very Long Baseline Interferometer (VLBI) observations as well as single-dish applications, both in continuum and spectroscopy. In order to assess the dynamic range of the new receiver chain, the presence at the SRT site of high-power interfering radio frequency signals from telecommunication services was surveyed by means of a mobile laboratory specifically designed for monitoring the Radio Frequency Interference (RFI) [3]. A signal centred at 5640 MHz emitted by weather radar was identified to be the most critical for the receiver linearity. The radar site was 50 km from the SRT and in line-of-sight. The power level of this signal reaching the SRT was measured to be around -50 dBm (assuming a 0 dBi antenna gain which is the standard value used when far-side lobes are considered). The radar frequency is slightly outside the nominal band of the receiver, and at these frequencies the passive components of the feed-system do not introduce any attenuation. The cryogenic ultra-sensitive Low Noise Amplifier (LNA) planned for this receiver is less robust than traditional LNAs and therefore more prone to linearity issues. The expected peak power level exceeds the linearity boundary of the LNA by about 10 dB and consequently it was decided to develop and install a planar microstrip High Temperature Superconductor (HTS) filter [4] before the LNA attenuating this interference by at least 20 dB.

Previous experiences demonstrated that HTS microwave filters are a valid option to mitigate RFI while minimizing additional ohmic losses, for instance around 0.1 dB for a P-band filter described in [5] and 0.15–0.25 dB for a C-band one [6]. The P-band HTS filters developed in 2010 are still fully operating at SRT, showing reliability characteristics over several years. From a design point of view, the new HTS filter here presented is more challenging due to the sharp transition in the transmission response. The filter design is based on six quarter-wave resonators coupled by capacitor pads and narrow gaps plus six spirals to produce the notch at 5640 MHz. An alternative design (cascaded triplet) has been also considered but then discarded due to the likely higher level of unwanted coupling and greater sensitivity to manufacturing errors.

Additionally, the experimental validation of the new set of HTS filters was performed by adopting a more accurate procedure with calibration done in the cryostat at the operation temperature. This results in a better agreement of the experimental matching response with the simulated data. However, the more significant improvement in the comparison between simulated and measured reflection coefficient is obtained by modelling the contact region between the circuit and the connector.

This paper starts from the filter specifications illustrated in Section 2, and then describes the electromagnetic design and fabrication in Section 3. Section 4 justifies the choice of a notch filter for the present application with respect to an alternative design. The experimental measurements performed in two different laboratories and with different calibration procedures are shown in Section 5 and compared with the simulated values. Finally, an improvement of the numerical model to explain some discrepancies in the matching response and the conclusions are reported in Sections 6 and 7 respectively.

2. Filter specifications

The main specification of the filter was to provide a very sharp transition between 5600 MHz, the maximum passband frequency, and the interference at 5640 MHz. Besides the interference central frequency, the filter was supposed to attenuate by 20 dB in a bandwidth of 10 MHz giving some margins for possible shifts of the radar central frequency (this attenuation mask is displayed in Fig. 5(b)). Additionally, since the LNA was designed to work between 4000 and 8000 MHz, the filter was also aimed at attenuating, without any specific mask, the frequencies outside the nominal pass band 4200-5600 MHz. A pass band above the notch was tolerated due to the lack of other strong interference in this frequency range. A list of the main electromagnetic specifications is reported in Table I. Three units were required, one for each linear polarization of the receiver plus one spare. Finally, a reasonable repeatability (not quantitatively described) in the responses of the three components was pursued.

Table I Specifications of HTS filter

Pass band (PB)	4200-5600 MHz
Reflection coefficient in PB	<-15 dB
Ohmic losses in PB	<0.25 dB
RFI Frequency	5640 MHz
RFI Attenuation	>20 dB

3. Filter design and fabrication

The filter was realized with Yttrium Barium Copper Oxide (YBCO) laid on a 0.5 mm thick Magnesium Oxide (MgO) substrate (electrical permittivity equal to 9.65).

The filter comprises 6 main resonators *1-6* in Fig. 1(a), forming a band-pass filter, chosen to be straight quarter-wave resonators coupled by capacitor pads and narrow gaps (Fig. 1(b)) because of their relatively high coupling, to make a wide pass band. They are not hairpins, to reduce coupling between non-adjacent resonators. The capacitor pads are relatively long and narrow, to allow a long and narrow box, which also reduces long-range coupling. A notch in the response is created by resonators *a-f* in Fig. 1(a), which are spirals, for their moderate level of coupling to the main resonators, and low coupling at larger distances, that is with each other. The longer pads also allow greater spacing of tuning screws for the spirals, but the screws were later found to be unnecessary. Resonators *a-f* in Fig. 1(a) are drawn above or below the main resonators to provide consistency with Fig. 1(b). Additionally, in Fig. 1(b) only slightly more than half of the filter is drawn because of the 180 degree rotational symmetry, with axis normal to the figure.

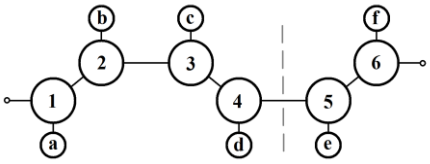

(a)

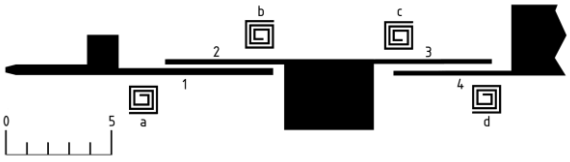

(b)

Fig. 1. ***(a)*** *Architecture of the notch filter;* ***(b)*** *geometrical layout of part of the filter. Slightly more than half geometry is drawn in (b), corresponding to the left of the dashed line in (a), due to its symmetry. The scale is given in mm*

Microwave filter design is well established, see e.g. [4] and [7]. An example specifically using quarter-wave resonators is given in [8]. Initially, for a filter with no notch, the required coupling coefficients are found as in [9], while the relationship between the coupling coefficients and the pad sizes and gaps are estimated from graphs based on e.m. simulations of pairs of resonators (using Sonnet [10]). The spirals are added, as described in [11] and [12]. Since a wide-band filter is being designed using narrow-band filter theory, adjustments using iterative simulations are inevitable; thus changes in target ripple and filter order, to improve the error margin, can be covered by the iterative changes. For example, moving from a 4^{th} to a 6^{th} order filter, the initial design can have $1/Q_e$ and k_{12} the same as the 4^{th} order filter, and k_{23}, k_{34} equal to the original k_{23}. The spiral winding direction is anti-clockwise (moving inwards), chosen by trial and error to give a flat pass band (at the expense of more ripple in

the upper pass band, which is irrelevant). The difference in response between clockwise and anticlockwise spirals is described further in [11].

The length of the resonators *1*, *2* and *3* are 7.325, 5.65 and 5.625 mm, and widths 0.325, 0.25 and 0.225 mm. The capacitor pads have dimensions 1.5x1.9 and 4.25x3.35 mm^2. The gap between resonator *1* and *2* is 0.175 mm, and between *3* and *4* it is 0.325 mm. Moreover, the six identical half-wavelength spiral resonators (total length equal to 9.9 mm and 0.1 mm width), each bent into a 1.35x1.375 mm^2 square, spaced from the main resonators with gaps of 0.5, 0.5, and 0.45 mm provide the stop band at 5640 MHz. The total dimensions of the filter are 41.5x9.5 mm^2, which means that in a 2-inch diameter wafer a maximum of three different circuits are obtainable. The outermost 0.5 mm of the input/output lines are tapered from a width of 0.5 to 0.25 mm to avoid unwanted contact with the carrier metallic walls. Additionally, the outermost 2 mm of the input/output lines were coated with 200 nm of gold (on top of the YBCO) to allow the electrical contact between the microstrip and the connector central pin.

The double-sided YBCO on MgO substrate, with the YBCO further coated with gold from which the external contacts were etched, was provided by CERACO, which was also responsible for the ion-beam milling and etching/cutting processes. Titanium carriers were fabricated and silver-plated to host the planar circuits (a gold over-layer was omitted due to the chemically benign environment in the vacuum chamber). Both activities have been contracted to external suppliers. The Anritsu sparkplug launcher K-connectors with sliding contacts have been used to connect the input/output microstrip lines.

The assembly of the filters was done in-house at INAF-IRA by using Ablefilm 5025E conducting adhesive film between the wafer and the carrier and Namics Sk60N conducting epoxy between the connector and the microstrip. The procedure was kept as similar as possible for the three filters to assure repeatability.

4. Comparison with cascaded triplet filters

Since the required notch is at the edge of the pass-band, a possible alternative is a filter containing cascaded triplets, whose transmission zeroes produce a very steep edge on one side of the pass-band (Fig. 2(a)) to reject the previously mentioned interfering signal. An obvious advantage in other applications is that it is does not have a spurious band to the right of the notch. It cannot be made arbitrarily small: as its width is decreased, the slope of S_{21} to the left of the notch decreases until there is little advantage over a plain Chebyshev filter.

A likely architecture is shown in Fig. 2(b). The transmission zeroes also cause the left-hand edge to be gentler, but a higher order filter (7th) partially compensates. A possible layout is given in Fig. 2(c), which includes half-wave resonators *1*, *4* and *7*, together with quarter-wave resonators *2*, *3*, *5* and *6*. The earlier in-line configuration of resonators *2* and *3* has been bent into a hair-pin to produce the cross coupling k_{13} between resonators *1* and *3*; the same applies for *5* and *6*. The difficulty is that the coupling between resonators such as *1* and *4*, or *2* and *4*, may become unacceptably large when the distance between the resonators is decreased, even though they are still not adjacent. Furthermore, the overall filter shape also necessitates a wider box, which may lead to lower frequency box modes, although it may not compare unfavourably against the present notch filter which also has quite low spurious modes. The transmission zero positions in the notch filter are determined by only one parameter, the resonant frequencies of the six spiral resonators, while with the cascaded triplets, it depends on cancellation of the signal in the path via resonators *1*, *2* and *3* by the signal in the direct path from *1* to *3*: several parameters are involved, so the notch position would be expected to be more prone to simulation or fabrication errors.

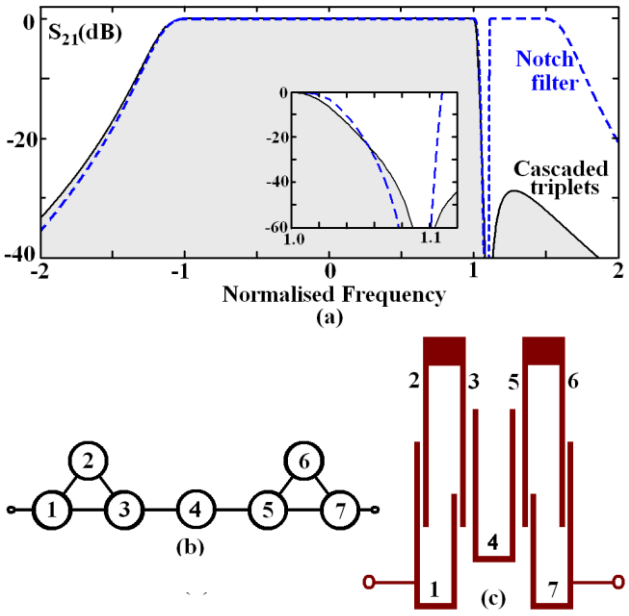

Fig. 2. ***(a)*** *Response of a possible filter containing cascaded triplets (solid black line) compared with the current notch filter (dashed blue), calculated from coupling matrices;* ***(b)*** *architecture and* ***(c)*** *a possible implementation of the cascaded triplet filter.*

The symmetrical notch filter is not designed as a 12th order filter, but much more simply as a 6th order band-pass filter with an added 6th order notch, where the pass band and notch characteristics are adjusted separately. The main resonators ideally all have the same resonant frequency, and there are four independent values of coupling coefficient (including the coupling to input and output) in the main path. The branch resonators (the spirals) have another resonant frequency, ideally equal coupling coefficients with the main resonators, giving a total of seven parameters to be found. The symmetrical cascaded triplet filter has five independent coupling coefficients. Five of the resonant frequencies are approximately equal, but resonators *2* and *6* are different; so there are at least seven parameters. The complexities are similar.

The normalised coefficients are given in Table II both for the notch filter and for the cascaded triplet filter. As seen in Fig. 2(a), the left-hand band edge slope is slightly inferior to the notch filter, although it can be improved by a higher filter order at the cost of greater complexity. The right-hand slope is also inferior below -30 dB but can be increased at the cost of a higher cross coupling term k_{13}; however it is already large and already results in a large side-lobe level of -29 dB. The worst-case sensitivity of ripple to errors in coupling coefficient is three times higher than the notch filter; this is the main disadvantage.

Finally, seven resonators would occupy less space than twelve, but this is not a major consideration in the present case, since both filters are very small. The notch filter is therefore competitive if the spurious pass band can be tolerated.

Table II Normalised coefficients for 6th order band pass plus notch (left column) and for the 7th order cascaded triplet (right column).

Band pass plus notch		Cascaded triplet	
$1/Q_e$	1.3123	$1/Q_e$	1.0829
k_{12}	1.0550	k_{12}	0.5418
k_{23}	0.7461	k_{23}	0.3000
k_{34}	0.7086	k_{34}	0.5766
$k_{1a}=k_{2b}=k_{3c}$	0.1900	k_{13}	-0.6803
$f_1=f_2=f_3$	0.2070	f_1	-0.0380
$f_a=f_b=f_c$	1.0920	f_2	0.8558
Notch width	0.111	f_3	-0.1367
Upper pass band width	0.389	f_4	-0.1024
Width of pass band to the left of notch	2		
Notes: Frequency is in normalised units. If pass band is scaled to 2 Hz, then all frequencies are in Hz. Ripple: 0.025 dB			

5. Experimental results

The first cycle of production of three filters was unsuccessful because: *i)* the silver plating peeled off the titanium carrier, likely due to a weak connection between the nickel flash and the titanium; *ii)* the conductive epoxy between the connector pins and the microstrip was very fragile and tended to crack during the cooling cycles. This latter issue was critical and probably due to a tolerance issue in the carrier fabrication which produced an additional vertical offset of 0.2 mm between the central pin of the connector and the microstrip layer. Part of one filter is shown in Fig. 3.

Therefore, new carriers and circuits were realized and assembled aimed at fixing the problems raised during the first cycle. In particular, in the new plating procedure a low thickness (1 μm) of nickel was used and the nickel activation was done in a gold bath. The thickness of the silver layer (5 μm) was chosen to be around five times the skin depth (calculated using the bulk resistivity of the silver at room temperature).

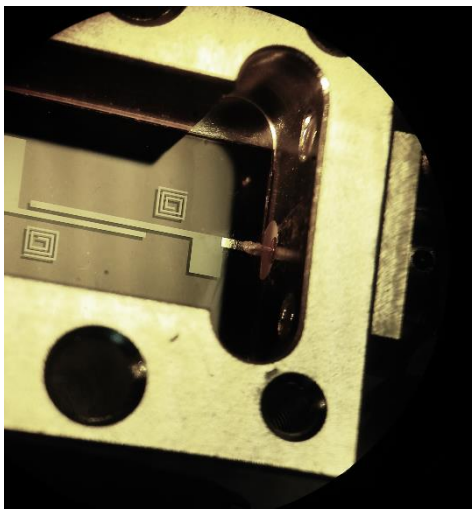

Fig. 3. *Part of one filter, fully assembled except for the cover (from the first set of filters, where SMA connectors were used; replaced by K connectors in the second set). The photograph has been processed to remove a golden tinge due to the illumination, and the contrast has been enhanced to show the superconducting layer.*

The three new filters survived the preliminary cooling cycles and therefore a full characterization was performed at 20 Kelvin. In order to increase the confidence in the results, the scattering parameters were measured in two INAF laboratories by using different hardware configurations both consisting on a Gifford-Mc Mahon cryostat connected to a Vector Network Analyser (VNA). Besides using different hardware and operators, the most important difference was in the VNA full-two-port error correction strategy: *i)* a Short-Open-Load-Thru (SOLT) procedure at room temperature inside the cryostat (at the filter's connector reference plane) followed by a "thru" adjustment at 20 K to take into account the lower losses in the internal coaxial lines at cryo-temperature (hereafter identified as 'warm_SOLT'); *ii)* each standard of the SOLT procedure was inserted sequentially inside the cryostat and cooled at cryo-temperature ('cold_SOLT'). The first approach is faster as it requires only two cooling cycles including the filter measurement, but it corrects only for the differences in amplitude of the transmission coefficient between room and cold temperatures. The second VNA strategy is formally more rigorous, as the standards are applied at the same conditions of the device under test; on the other hand, it needs five separate cooling cycles and therefore can suffer of drifts in the VNA. However, in order to take into account variations in the amplitude of the transmission coefficient, a "thru" was measured again after the filter (sixth cooling cycle).

The main experimental results are compared with the Sonnet data (assuming an ideal 50 ohm port and accurate fine/edge meshing with a cell size of 6.25 μm) and summarized in Figs. 4 and 5. In particular, Fig. 4 shows the reflection coefficient results with measurements performed with the VNA calibrated at room temperature (Fig. 4(a)) and at 20 Kelvin (Fig. 4(b)). For each plot, the grey region is obtained by taking, for each frequency, the maximum and minimum value for the three filters at the two ports ($|S_{11}|$ and $|S_{22}|$). This gives a range which can be compared with the expected Sonnet results. The two sets of measurements (warm_SOLT and cold_SOLT) show that at the higher frequency (from the peak centred at 5000 MHz) a good correspondence in the response is obtained, while at lower frequency the simulated first two peaks are well aligned only with the cold_SOLT data. As far as the matching level is concerned, we notice, for both sets of experimental data, a 5 dB offset between measurements and numerical response. This discrepancy will be discussed in Section 6. However, the worst measured value in the 4200-5600 MHz range is within the specification being -15.6 dB for both sets and it is positioned in the steep slope around 5600 MHz. Looking at the central part of the band, we notice that the maximum of the third peak is -15.7 dB and -16.8 dB for the warm_SOLT and cold_SOLT data respectively.

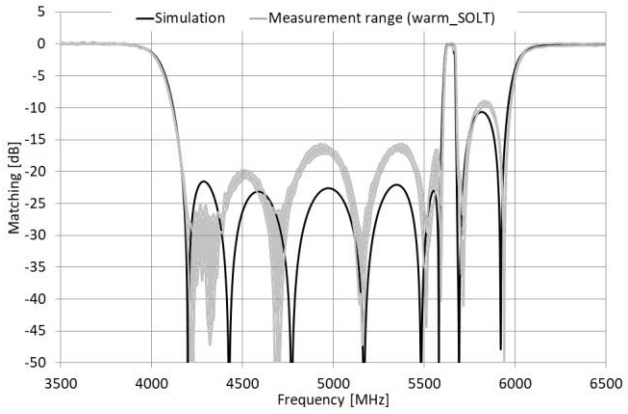

(a)

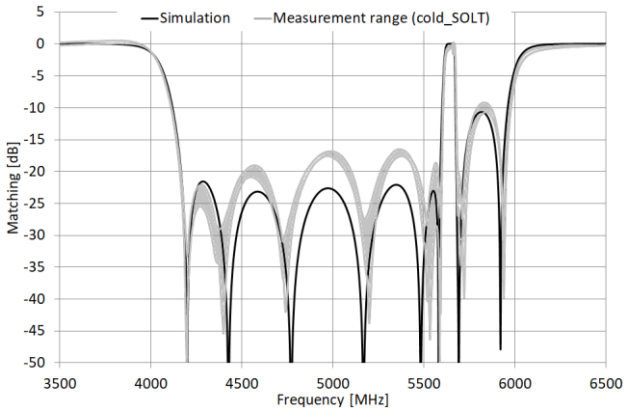

(b)

Fig. 4. *Measured and simulated matching with two different strategies in the VNA calibration:* ***(a)*** *at room temperature (warm_SOLT);* ***(b)*** *at 20 Kelvin (cold_SOLT).*

The measured transmission coefficients (average between $|S_{12}|$ and $|S_{21}|$) for the three filters are plotted in the pass band in Fig. 5(a) together with the simulated response. The simulated transmission coefficient is computed by using a resistor model to consider the losses of the HTS assumed equal to 2e-5 ohms/sq. As expected, the measured losses are much higher than those numerically computed since they are dominated by the epoxy and the connector, which are not included in the Sonnet model. The two sets of measured data (warm_SOLT and cold_SOLT) agree quite well, we notice only a slight difference, less than 0.05 dB. Generally speaking, the ohmic losses (corresponding to the maxima of the curves) vary between 0.15-0.20 dB (depending on the filter) at lower frequency and 0.20-0.25 dB at higher frequency. The filter responses, and in particular those of filter #2 and #3, agree very well and demonstrate an excellent repeatability.

One of the most important results is the notch response which is plotted in Fig. 5(b). The desired specification was reached, having an attenuation between -30 and -40 dB at 5640 MHz depending on the filter, despite the slight shift with respect to the simulated values of 2 MHz downwards for filter #1 and 3 MHz upwards for filters #2 and #3. The corners in Fig. 5(b) indicate the attenuation mask required by the filter specification.

Finally, the plot in Fig. 5(c) shows the measured transmission coefficient in a very wide frequency range (2-20 GHz). Apart from the notch, the simulated -3 dB cut-off frequencies of the pass-band are at 4047 and 6012 MHz, while the measured ones are 4043 and 6017 MHz for the three filters. The high order harmonics, which start at 11 GHz, agree very well between simulation and measured data up to 15 GHz. Some discrepancies emerge at higher frequencies. For the notch and wide-band transmission responses, the agreement between the data obtained from the two calibration strategies is so good that only one set is plotted.

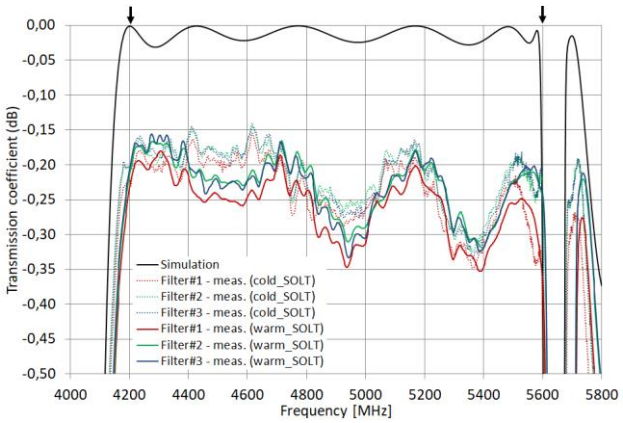

(a)

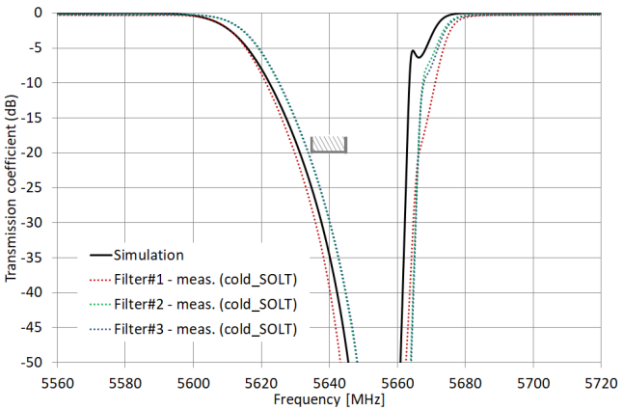

(b)

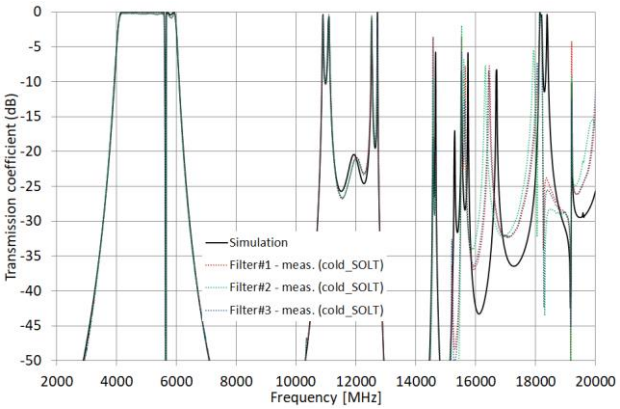

(c)

Fig. 5. *Measured and simulated transmission coefficient:* ***(a)*** *in the nominal band with two different strategies of VNA calibration (warm_SOLT and cold_SOLT);* ***(b)*** *in the stop band (cold_SOLT);* ***(c)*** *up to 20 GHz (cold_SOLT). The black arrows in (a) indicate the frequencies of the nominal pass band, while the grey corners in (b) show the required attenuation mask at the notch frequency.*

6. Insights in the simulated matching response

The results shown in Section 5 shows an overall good agreement between simulations and measurements. However, this is only approximately true for the matching response, which is a very sensitive parameter below -15 dB. The cold_SOLT measured data (Fig. 4(b)) agree more than the warm_SOLT ones (Fig. 4(a)) with the numerical response, even if they show a deterioration in the level not predicted by the simulator. The idea was that this discrepancy could be due to the transition region between the coaxial connector and the microstrip, which was not modelled in the simulator. Therefore, the original circuit in Sonnet was modified according to a more realistic geometry of the transition. In particular, a 3D block (2x0.5x0.15 mm^3 LxWxH) was introduced in the input/output lines to take into account the presence of the epoxy and the connector structure, for an estimated overall thickness of 0.15 mm, see Fig. 6(a). The main spurious effect of the epoxy and the connector pin is to add a capacitive effect between the metallic wall of the enclosure box and the vertical surface of the simulated block (distance between the two capacitor plates equal to 0.5 mm). Being interested in the matching response, rather than in the losses, the 3D block was assumed to be a perfect electrical conductor. The new simulated data (black dashed curve) are plotted in Fig. 6(b) together with the original simulation (black continuous curve) and with the cold_SOLT measured results (grey region). It is evident from the second, third and fourth peaks that the matching level increases in the simulated response of the new geometry (with glue) with respect to the ideal planar configuration. The new curve matches very well with the cold_SOLT data, recovering the previous offset.

This result suggests that for future filter designs, it is highly recommendable to model, even in a quite simplistic way, the presence of the connector pin and epoxy drop during the Sonnet optimization process to better predict the final response of the filter.

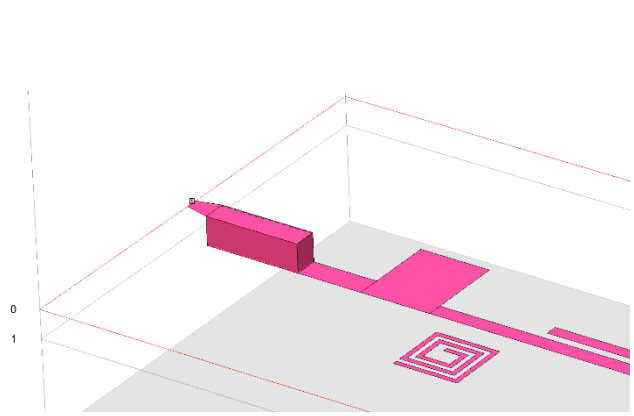

(a)

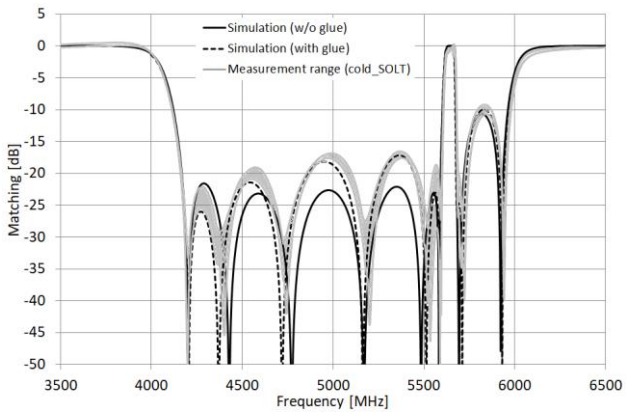

(b)

Fig. 6. (a) *Geometry of the contact region between connector and microstrip as implemented in Sonnet (the distance in the vertical direction between layer 1 and layer 0 is 0.15 mm);* ***(b)*** *measured (cold_SOLT) and simulated (with and without modelling the contact region) matching responses.*

7. Conclusions

In order to mitigate interference from a weather radar, a very sharp microwave filter has been developed for the Sardinia Radio Telescope. The filter aims to transmit the frequency range 4200-5600 MHz and attenuate by at least 20 dB at 5640 MHz. A High Temperature Superconductor material was used to implement this filter. The scattering parameters characterization at 20 Kelvin showed values according to the requirements. The cryo-cooled measurements were repeated in two labs with different VNA calibration strategies and they resulted in a good agreement especially in terms of the transmission coefficient. The approach of calibrating the VNA at 20 Kelvin provides matching results more similar to the simulations than the room temperature calibration plus "thru" correction. Finally, a further investigation has been conducted to better simulate the contact region between the circuit and the connector: this results in a significant improvement in the agreement with the measured response. Therefore, in future filter designs the electromagnetic analysis should take into account the contact region for improving the numerical results.

8. Acknowledgments

The authors wish to thank Luca Carbonaro from the INAF - Arcetri Astrophysical Observatory for providing useful suggestions on the mechanical design and Richard Prestage from the Green Bank Observatory for his valuable comments on the contents of the article. Finally, the authors are grateful to the Italian company Galvanelettronica Electroplating for putting a lot of R&D efforts in the plating process of the titanium carriers.

9. References

[1] http://www.srt.inaf.it/
[2] Bolli, P., Orlati, A., Stringhetti, L., et al., 'Sardinia Radio Telescope: General Description, Technical Commissioning and First Light', *Journal of Astronomical Instrumentation*, **4** (3-4) (2015)
[3] Bolli, P., Gaudiomonte, F., Ambrosini, R., et al., 'The Mobile Laboratory for Radio Frequency Interference monitoring at the Sardinia Radio Telescope', *IEEE Antennas and Propagation Magazine*, **55** (5), 19-24 (2013)
[4] Hong, J.-S. G., Lancaster, M. J., Microstrip Filters for RF/Microwave Applications, ed. Chang, K., John Wiley and Sons, Inc. (2001)
[5] Bolli, P., Huang, F., 'Superconducting filter for radio astronomy using interdigitated, capacitively loaded spirals', *Experimental Astronomy*, **33** (1), 225–236 (2012)
[6] Bolli, P., Cresci, L., Huang, F., Mariotti, S., Panella, D., 'A high temperature superconductor microwave filter working in C-band for the Sardinia Radio Telescope', *Journal of Astronomical Instrumentation*, **3** (1), (2014)
[7] Cameron, J.C., Kudsia, C.M., Mansour, R.R., Microwave Filters for Communication Systems, John Wiely and Sons, Inc, (2007)
[8] Huang, F. 'Suppression of harmonics in Microstrip Filters Using a Combination of Techniques', *IEEE Trans. Microw. Theory Techn.*, **63** (10), 3453-3461 (2015)
[9] Matthaei, G., Young, L., Jones, E.M.T., Microwave Filters, Impedance-Matching Networks, and Coupling Structures, Artech House, pp. 100 and 432 (1980)
[10] http://www.sonnetsoftware.com/
[11] Huang, F., 'Dual-band superconducting spiral filters including narrow band-stop notches', *IEEE Trans. Microwave Theory and Techn.*, **57** (5), 1188-1195 (2009)
[12] Macchiarella, G., Tamiazzo, S., 'Design techniques for dual-passband filters', *IEEE Trans. Microwave Theory and Techn.*, **53** (11), 3265-3271 (2005)